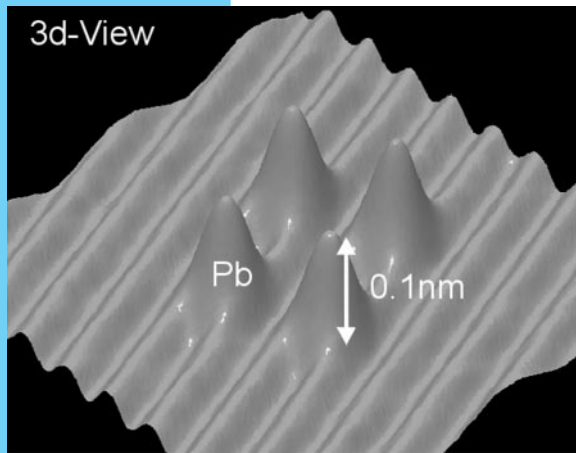


PART O N E

CHAPTER 2

Atomic Bonding



The scanning tunneling microscope (Section 4.7) allows the imaging of individual atoms bonded to a material surface. In this case, the microscope was also used to manipulate the atoms into a simple pattern. Four lead atoms are shown forming a rectangle on the surface of a copper crystal. (From G. Meyer and K. H. Rieder, MRS Bulletin 23 28 [1998].)

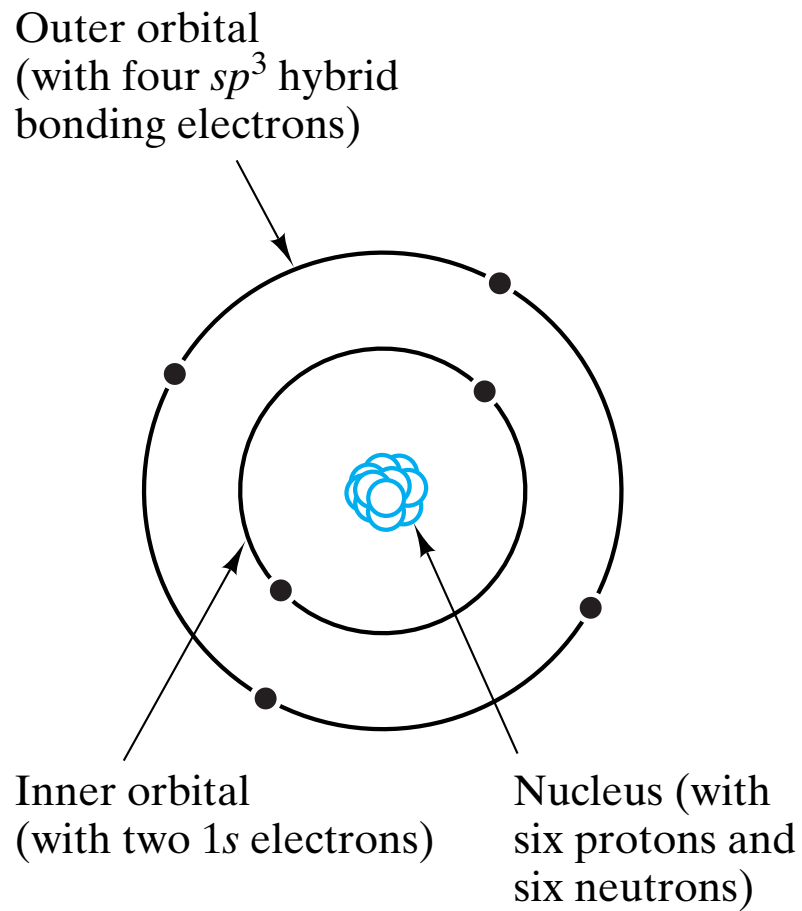


Figure 2-1 Schematic of the planetary model of a ^{12}C atom.

I A																	0	
1 H 1.008	II A											III A	IV A	V A	VIA	VII A	2 He 4.003	
3 Li 6.941	4 Be 9.012											5 B 10.81	6 C 12.01	7 N 14.01	8 O 16.00	9 F 19.00	10 Ne 20.18	
11 Na 22.99	12 Mg 24.31	III B	IV B	V B	VIB	VII B	VIII				IB	II B	13 Al 26.98	14 Si 28.09	15 P 30.97	16 S 32.06	17 Cl 35.45	18 Ar 39.95
19 K 39.10	20 Ca 40.08	21 Sc 44.96	22 Ti 47.90	23 V 50.94	24 Cr 52.00	25 Mn 54.94	26 Fe 55.85	27 Co 58.93	28 Ni 58.71	29 Cu 63.55	30 Zn 65.38	31 Ga 69.72	32 Ge 72.59	33 As 74.92	34 Se 78.96	35 Br 79.90	36 Kr 83.80	
37 Rb 85.47	38 Sr 87.62	39 Y 88.91	40 Zr 91.22	41 Nb 92.91	42 Mo 95.94	43 Tc 98.91	44 Ru 101.07	45 Rh 102.91	46 Pd 106.4	47 Ag 107.87	48 Cd 112.4	49 In 114.82	50 Sn 118.69	51 Sb 121.75	52 Te 127.60	53 I 126.90	54 Xe 131.30	
55 Cs 132.91	56 Ba 137.33	57 La 138.91	72 Hf 178.49	73 Ta 180.95	74 W 183.85	75 Re 186.2	76 Os 190.2	77 Ir 192.22	78 Pt 195.09	79 Au 196.97	80 Hg 200.59	81 Tl 204.37	82 Pb 207.2	83 Bi 208.98	84 Po (210)	85 At (210)	86 Rn (222)	
87 Fr (223)	88 Ra 226.03	89 Ac (227)																

58 Ce 140.12	59 Pr 140.91	60 Nd 144.24	61 Pm (145)	62 Sm 150.4	63 Eu 151.96	64 Gd 157.25	65 Tb 158.93	66 Dy 162.50	67 Ho 164.93	68 Er 167.26	69 Tm 168.93	70 Yb 173.04	71 Lu 174.97
90 Th 232.04	91 Pa 231.04	92 U 238.03	93 Np 237.05	94 Pu (244)	95 Am (243)	96 Cm (247)	97 Bk (247)	98 Cf (251)	99 Es (254)	100 Fm (257)	101 Md (258)	102 No (259)	103 Lw (260)

Figure 2-2 Periodic table of the elements indicating atomic number and atomic mass (in amu).

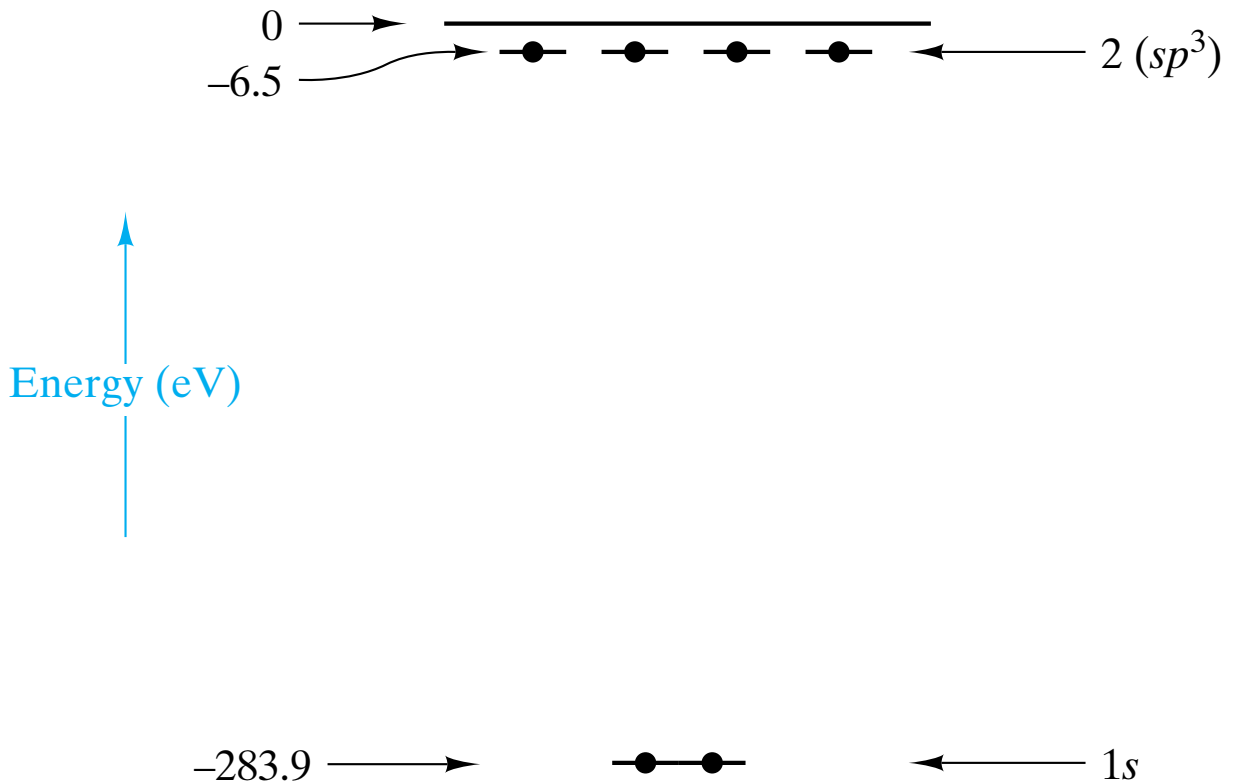


Figure 2-3 Energy-level diagram for the orbital electrons in a ^{12}C atom. Notice the sign convention. An attractive energy is negative. The $1s$ electrons are closer to the nucleus (see Figure 2-1) and more strongly bound (binding energy = -283.9 eV). The outer orbital electrons have a binding energy of only -6.5 eV. The zero level of binding energy corresponds to an electron completely removed from the attractive potential of the nucleus.

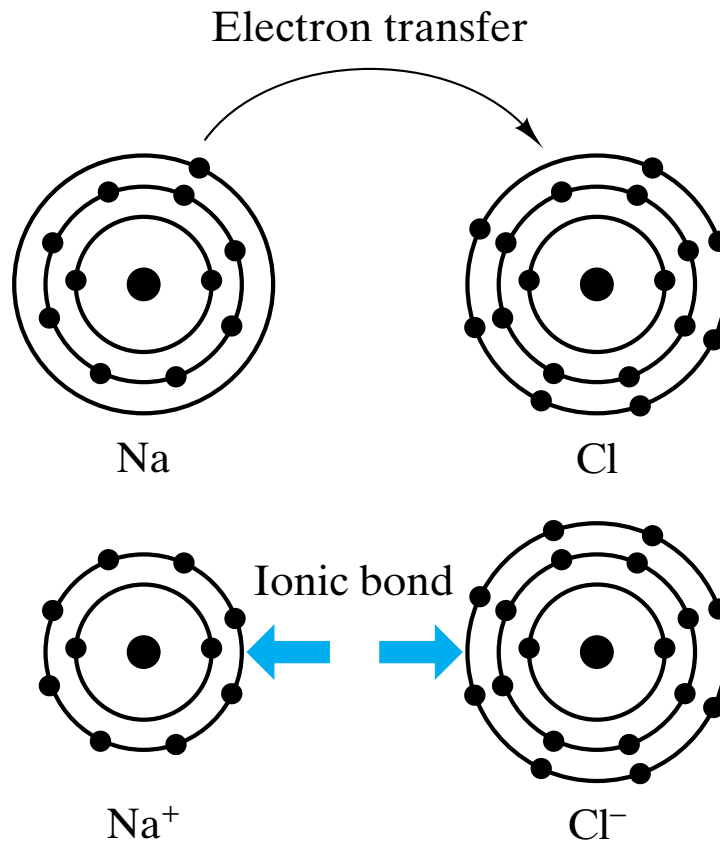


Figure 2-4 *Ionic bonding between sodium and chlorine atoms. Electron transfer from Na to Cl creates a cation (Na⁺) and an anion (Cl⁻). The ionic bond is due to the coulombic attraction between the ions of opposite charge.*

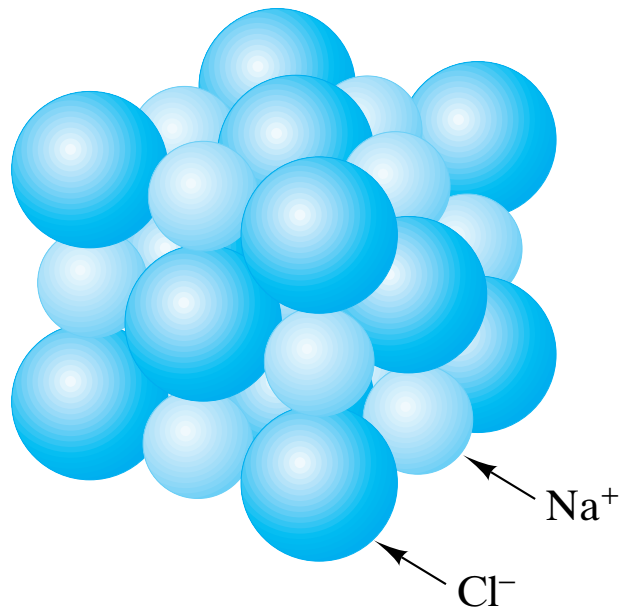


Figure 2-5 *Regular stacking of Na^+ and Cl^- ions in solid NaCl . This is indicative of the nondirectional nature of ionic bonding.*

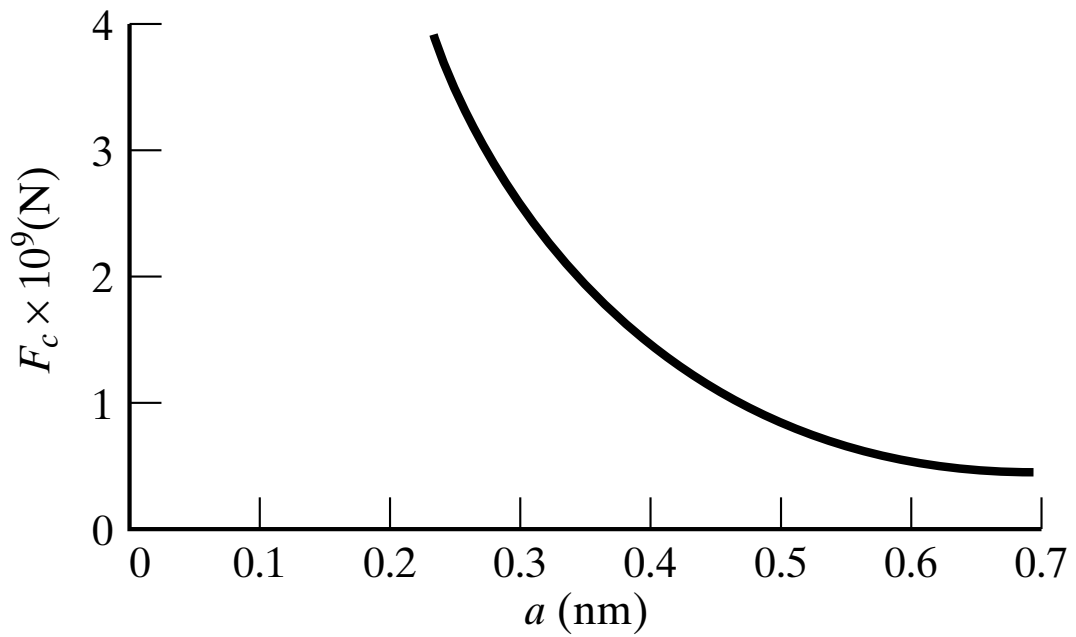
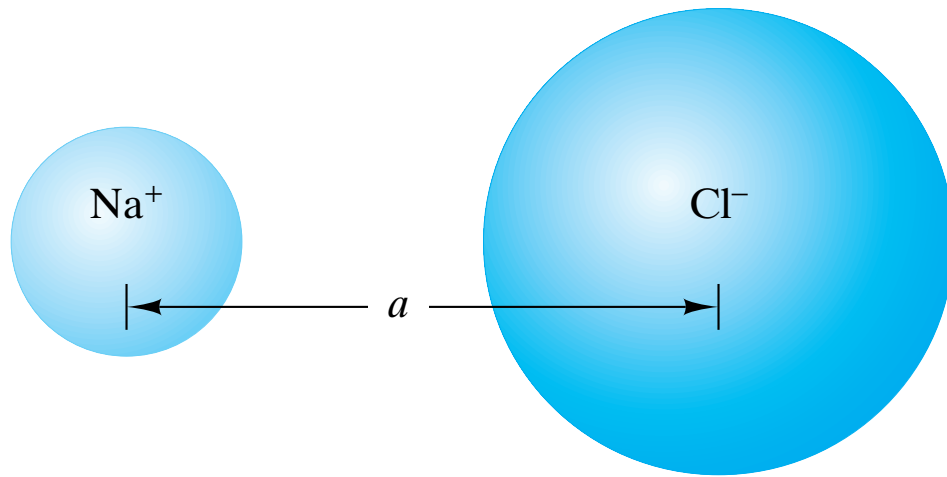


Figure 2-6 Plot of the coulombic force (Equation 2.1) for a Na^+ — Cl^- pair.

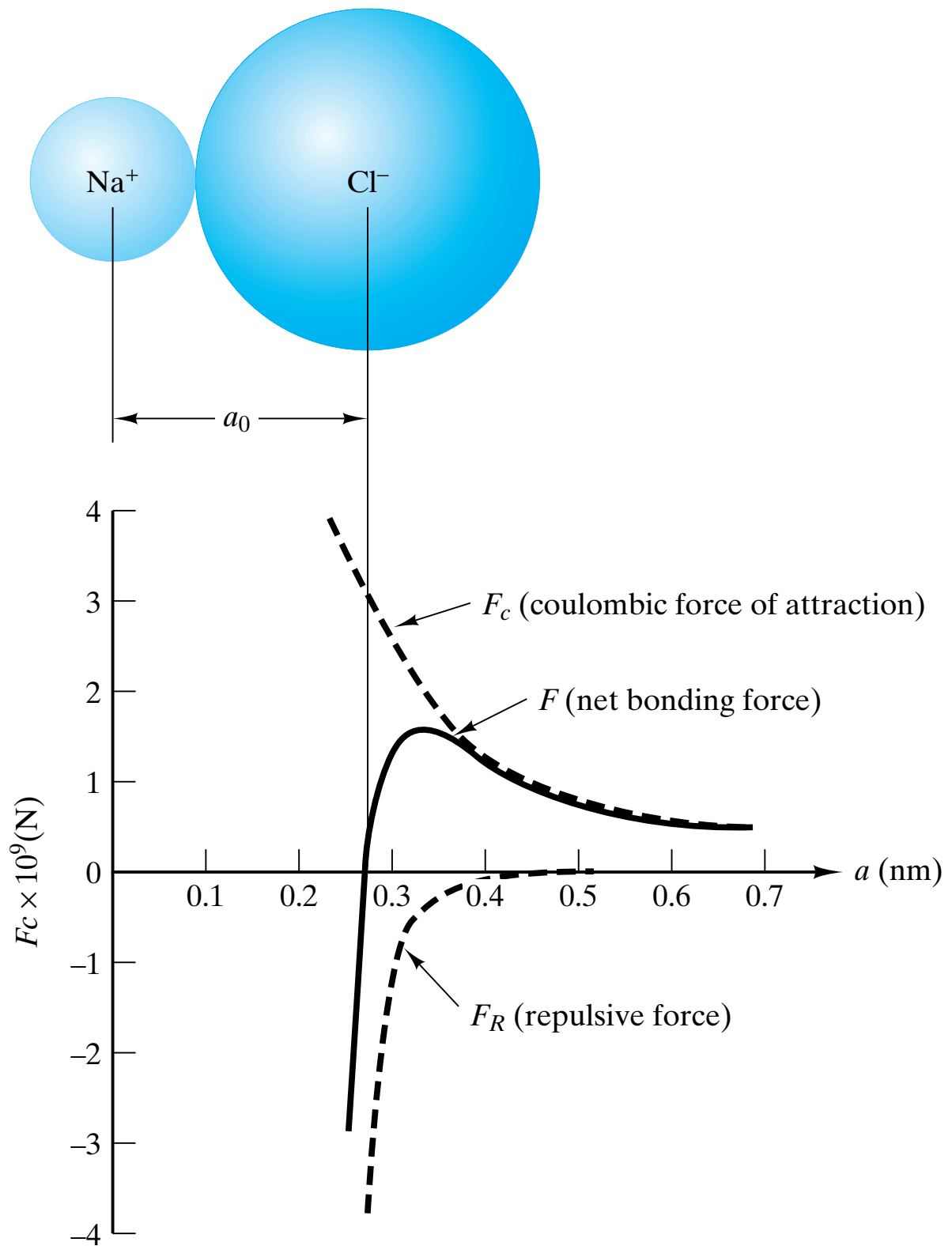


Figure 2-7 Net bonding force curve for a $\text{Na}^+ - \text{Cl}^-$ pair showing an equilibrium bond length of $a_0 = 0.28$ nm.

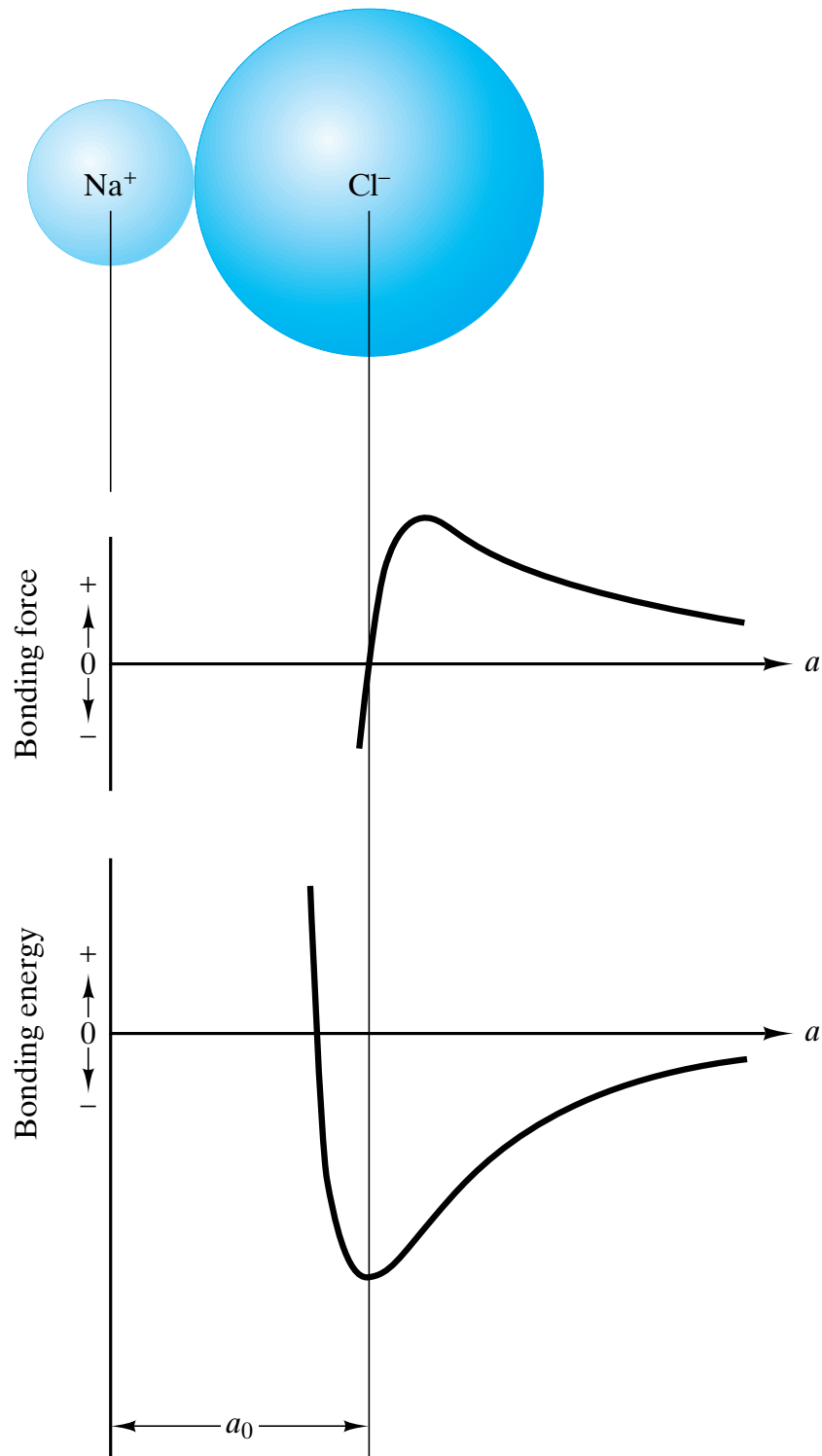


Figure 2-8 Comparison of the bonding force curve and the bonding energy curve for a $\text{Na}^+ - \text{Cl}^-$ pair. Since $F = dE/da$, the equilibrium bond length (a_0) occurs where $F = 0$ and E is a minimum (see Equation 2.5).

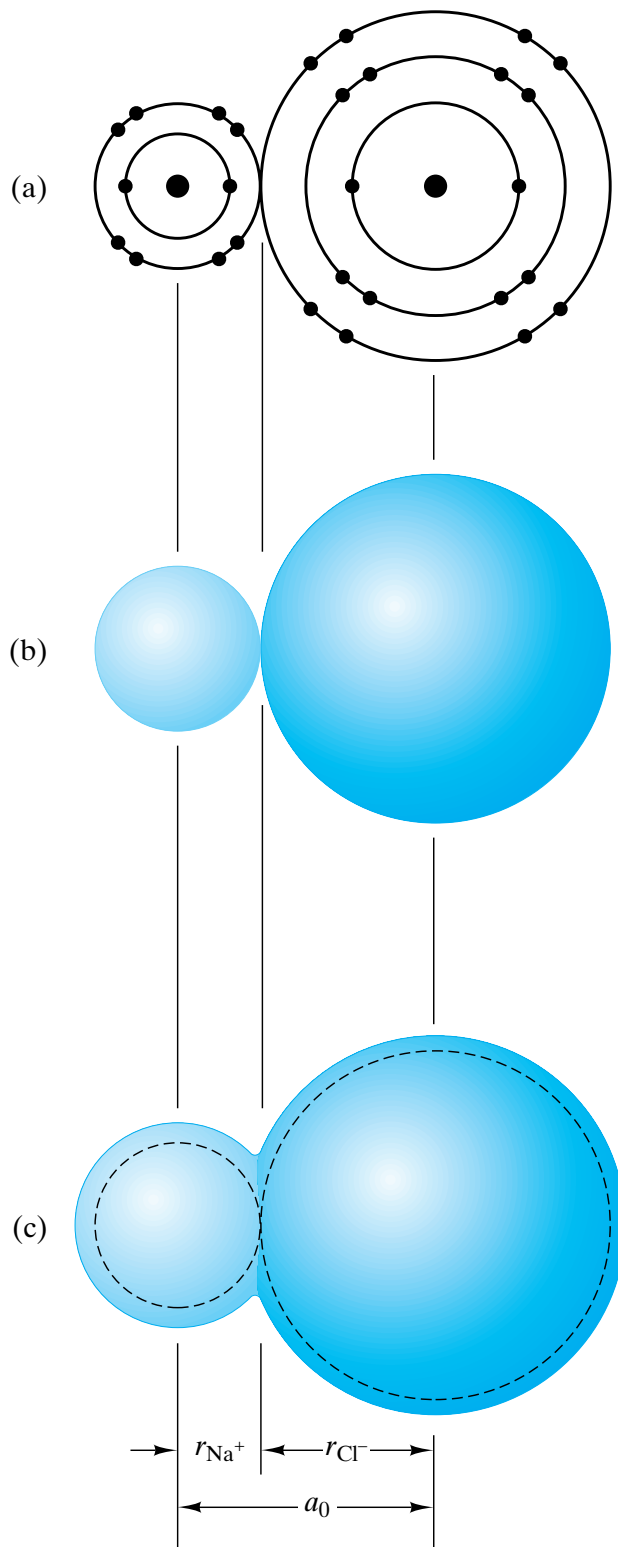


Figure 2-9 Comparison of (a) a planetary model of a $\text{Na}^+ - \text{Cl}^-$ pair with (b) a hard-sphere model and (c) a soft-sphere model.

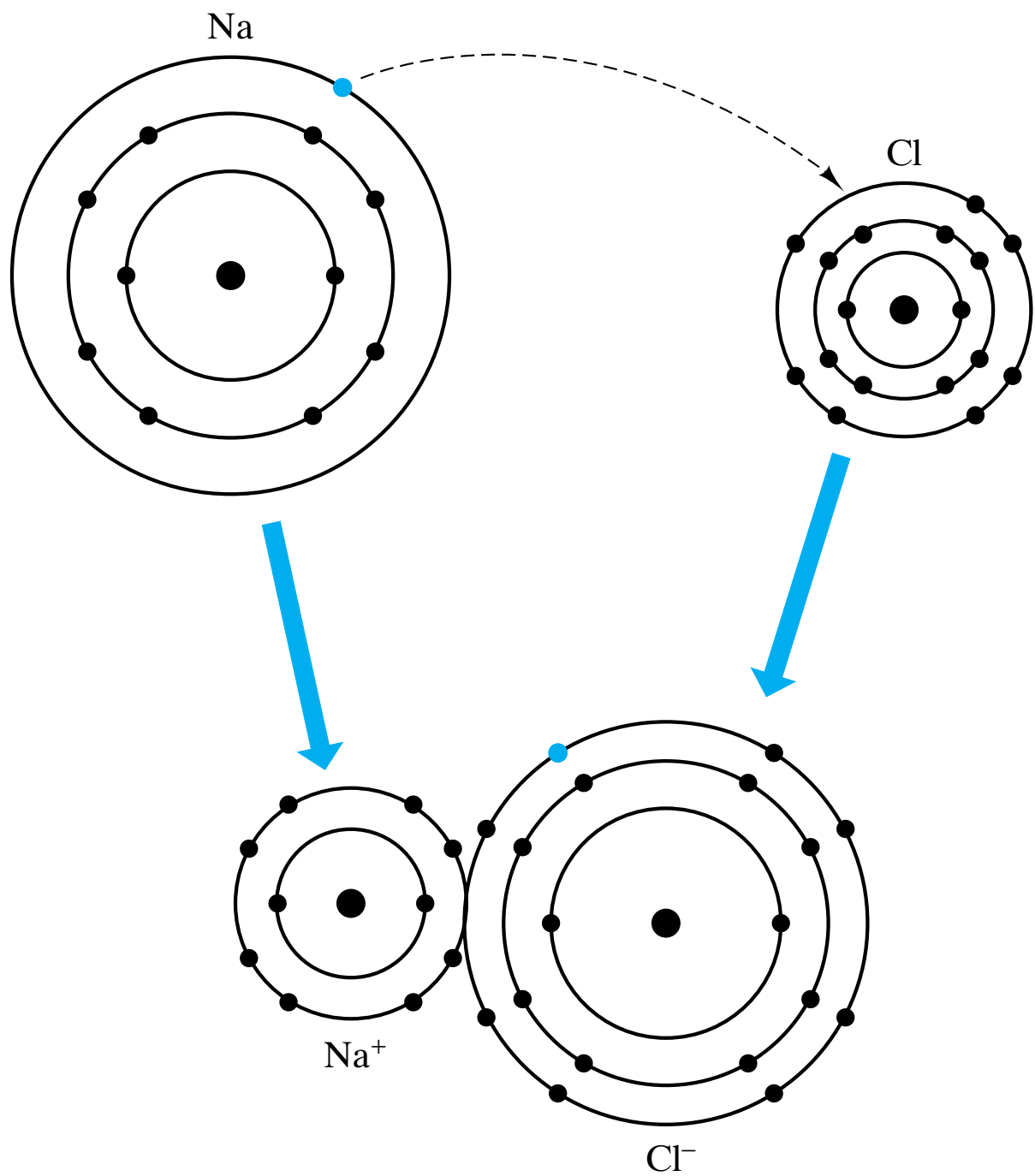


Figure 2-10 Formation of an ionic bond between sodium and chlorine in which the effect of ionization on atomic radius is illustrated. The cation (Na^+) becomes smaller than the neutral atom (Na), while the anion (Cl^-) becomes larger than the neutral atom (Cl).

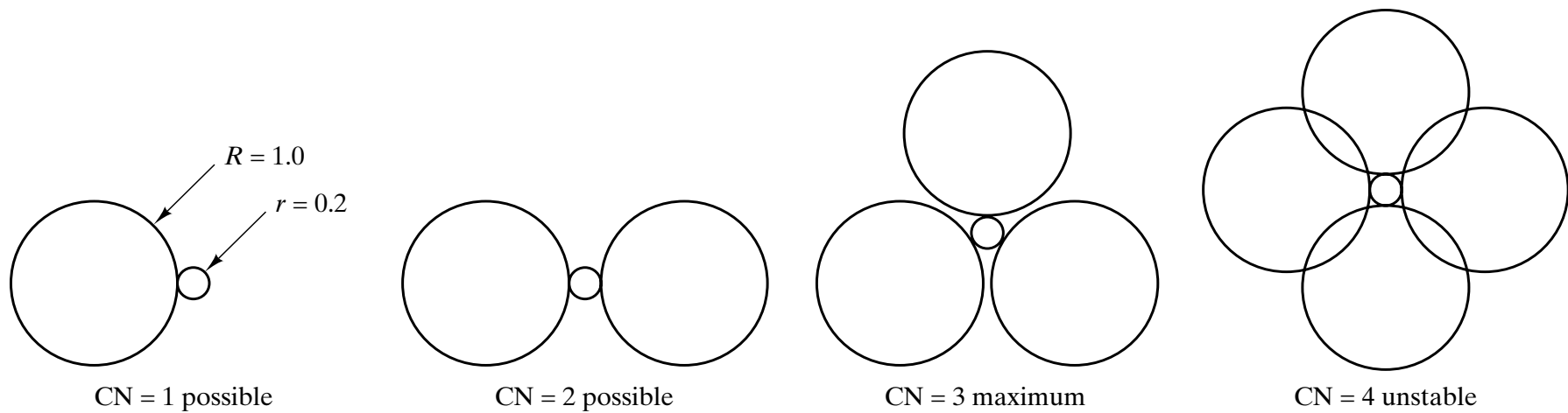


Figure 2-11 *The largest number of ions of radius R that can coordinate an atom of radius r is 3 when the radius ratio, $r/R = 0.2$. (Note: The instability for $CN = 4$ can be reduced but not eliminated by allowing a three-dimensional, rather than a coplanar, stacking of the larger ions.)*

$$\cos 30^\circ = 0.866 = \frac{R}{r + R} \rightarrow \frac{r}{R} = 0.155$$

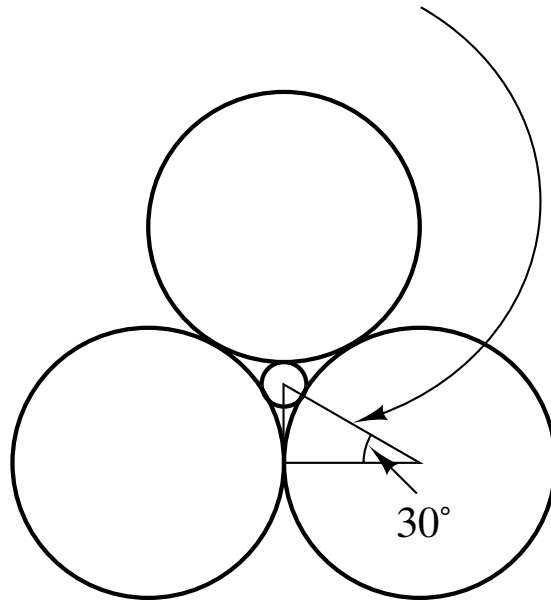
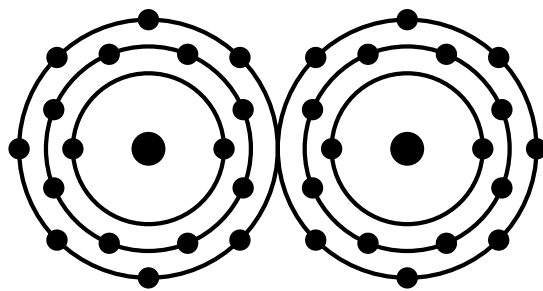
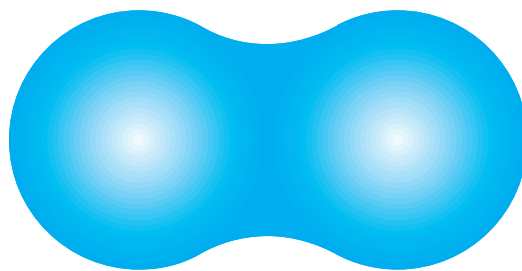


Figure 2-12 *The minimum radius ratio, r/R , that can produce threefold coordination is 0.155.*



(a)



(b)

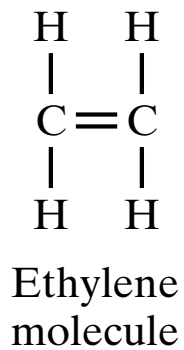


(c)

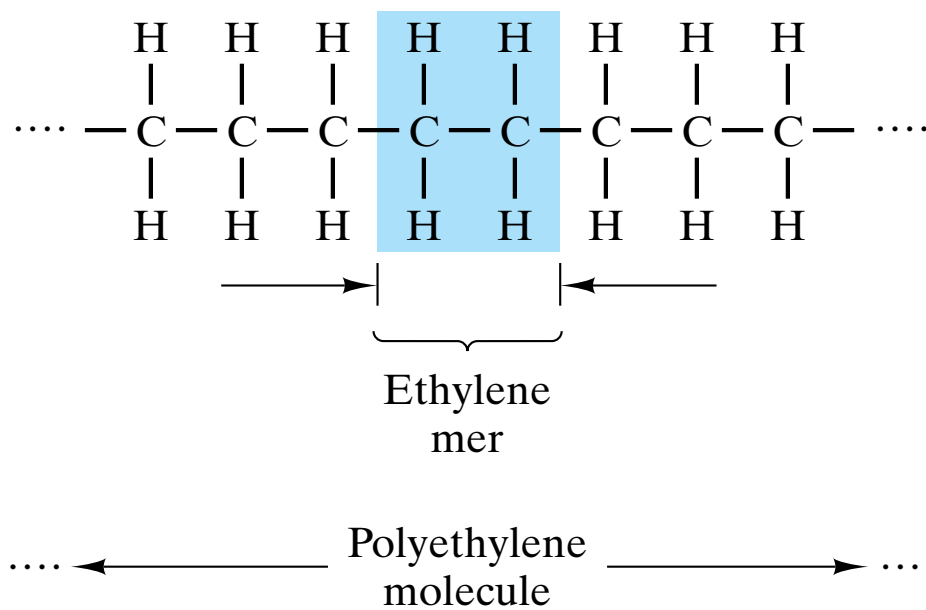


(d)

Figure 2-13 *The covalent bond in a molecule of chlorine gas, Cl_2 , is illustrated with (a) a planetary model compared with (b) the actual electron density and (c) an “electron-dot” schematic and (d) a “bond-line” schematic.*



(a)



(b)

Figure 2-14 (a) An ethylene molecule (C_2H_4) is compared with (b) a polyethylene molecule $(-\text{C}_2\text{H}_4-)_n$ that results from the conversion of the $\text{C}=\text{C}$ double bond into two $\text{C}-\text{C}$ single bonds.

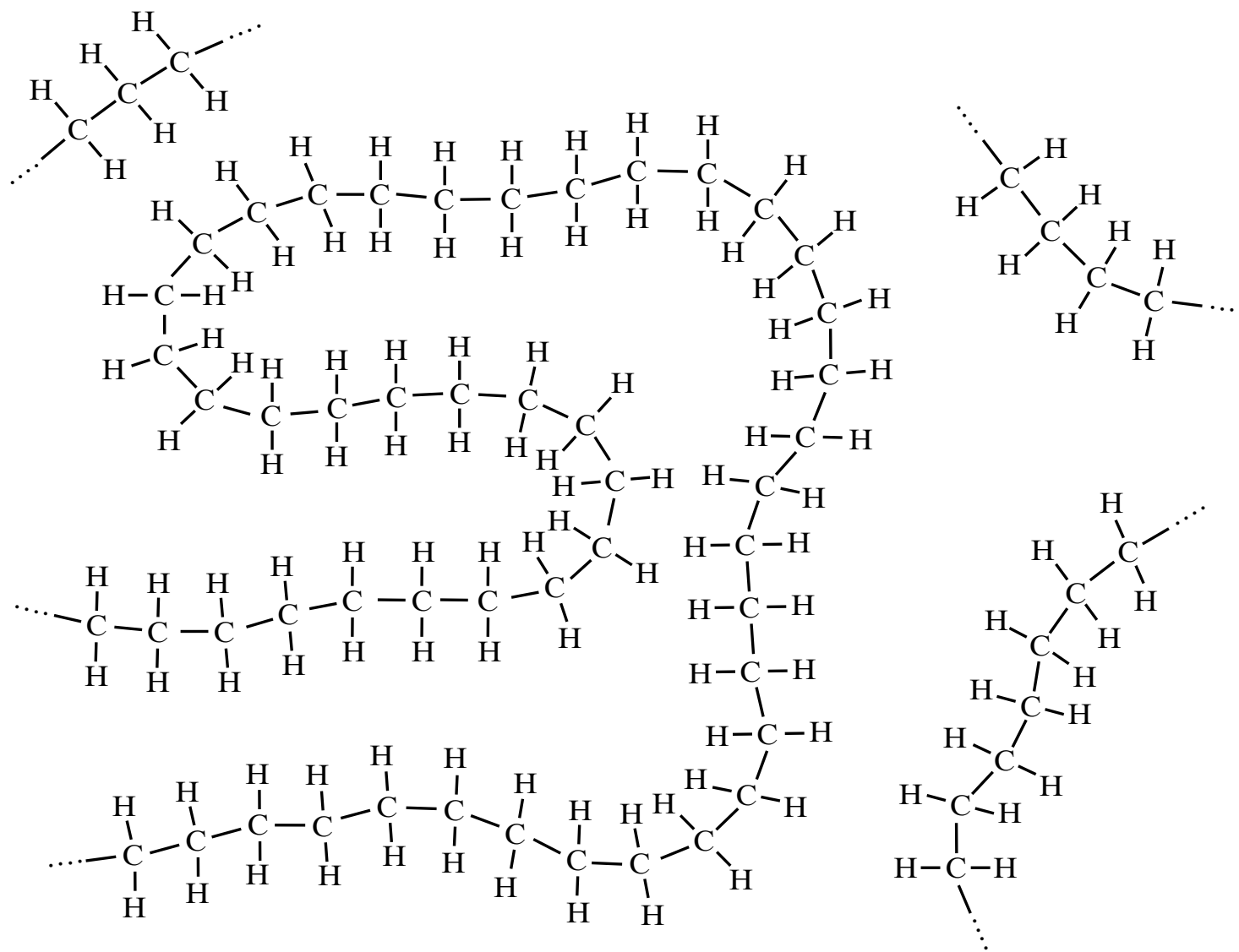


Figure 2-15 Two-dimensional schematic representation of the “spaghettilike” structure of solid polyethylene.

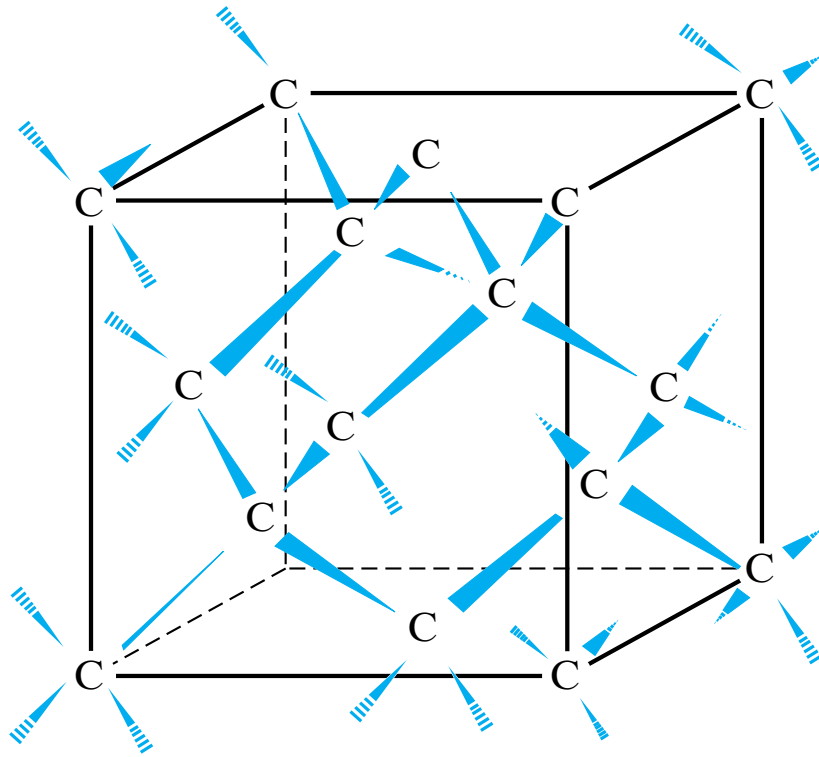


Figure 2-16 *Three-dimensional structure of bonding in the covalent solid, carbon (diamond). Each carbon atom (C) has four covalent bonds to four other carbon atoms. (This geometry can be compared with the “diamond cubic” structure of Figure 3–23.) In this illustration, the “bond-line” schematic of covalent bonding is given a perspective view to emphasize the spatial arrangement of bonded carbon atoms.*

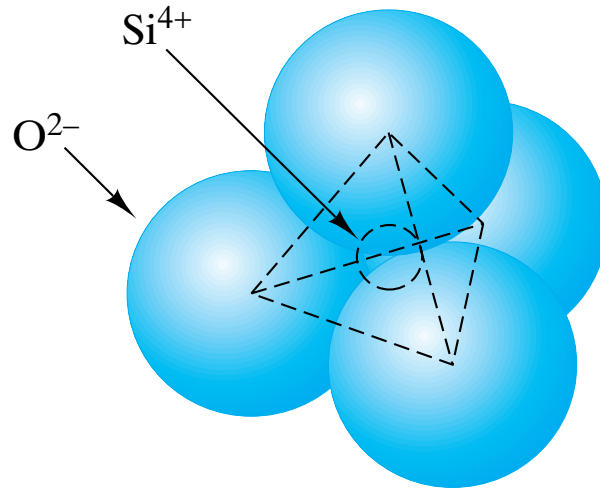


Figure 2-17 *The SiO_4^{4-} tetrahedron represented as a cluster of ions. In fact, the Si—O bond exhibits both ionic and covalent character.*

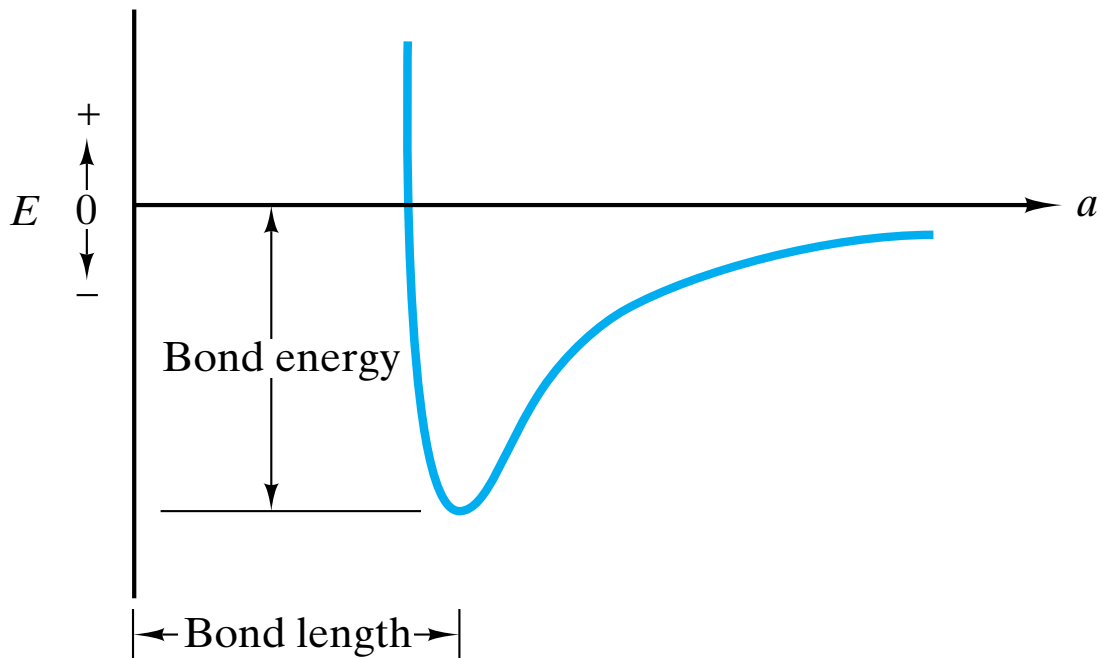


Figure 2-18 *The general shape of the bond energy curve as well as associated terminology applies to covalent as well as ionic bonding. (The same is true of metallic and secondary bonding.)*

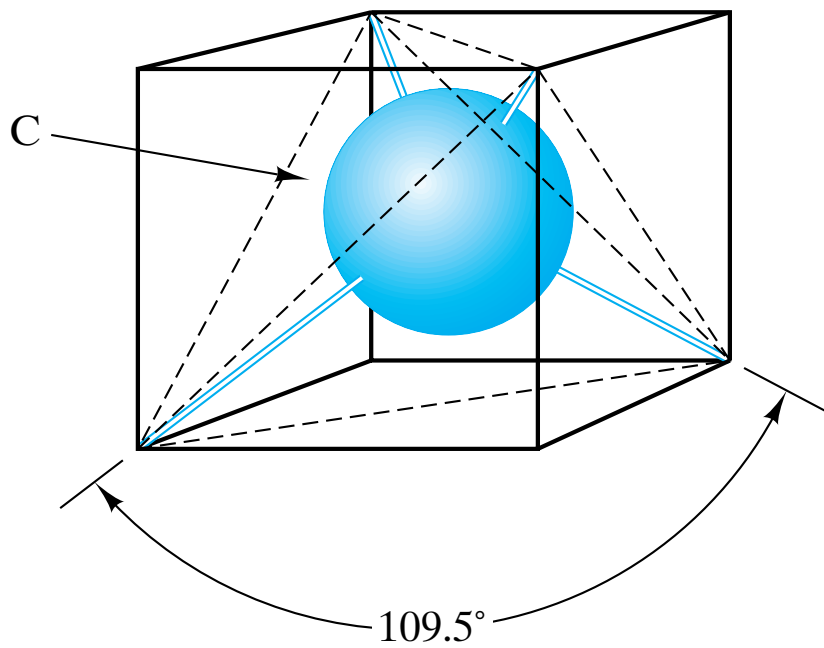
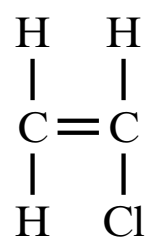
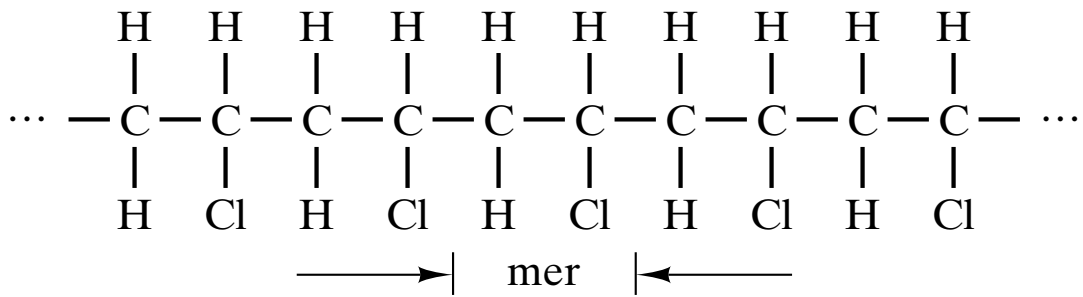
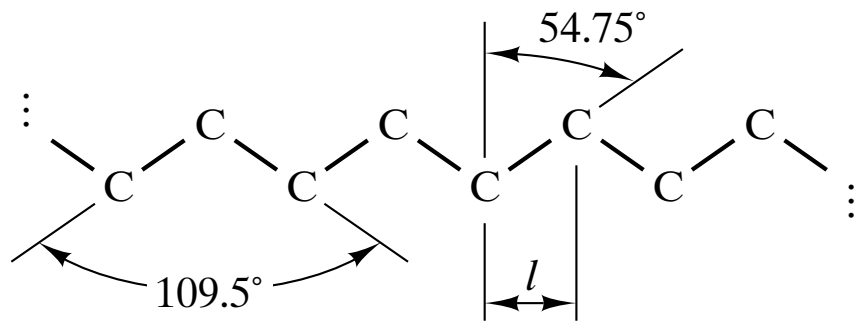


Figure 2-19 *Tetrahedral configuration of covalent bonds with carbon. The bond angle is 109.5° .*







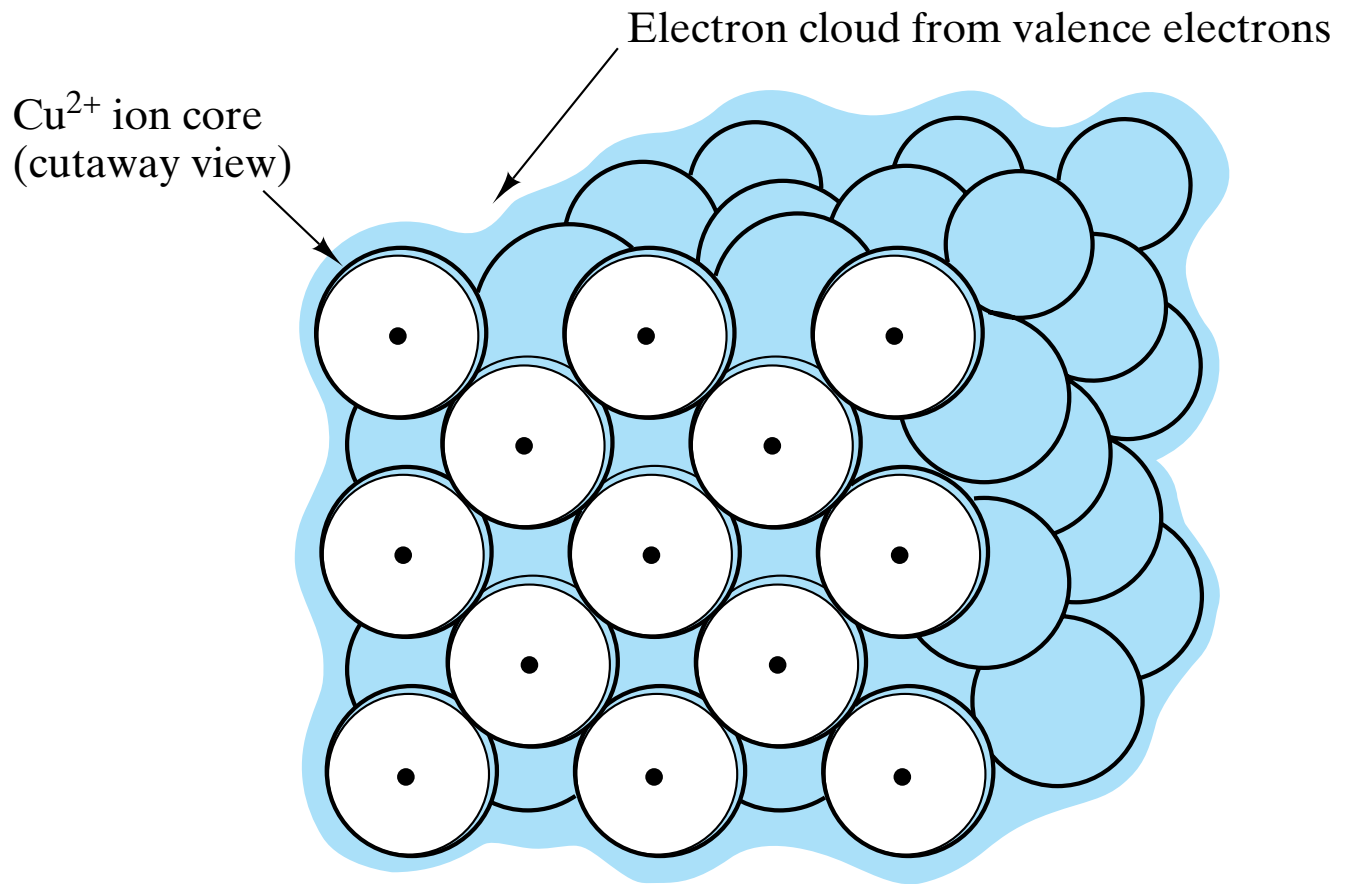


Figure 2-20 *Metallic bond consisting of an electron cloud, or gas. An imaginary slice is shown through the front face of the crystal structure of copper, revealing Cu^{2+} ion cores bonded by the delocalized valence electrons.*

I A																	0		
1 H 2.1																	2 He -		
II A												III A	IV A	V A	VIA	VIIA			
3 Li 1.0	4 Be 1.5											5 B 2.0	6 C 2.5	7 N 3.0	8 O 3.5	9 F 4.0	10 Ne -		
11 Na 0.9	12 Mg 1.2	III B	IV B	V B	VI B	VII B	VIII					I B	II B	13 Al 1.5	14 Si 1.8	15 P 2.1	16 S 2.5	17 Cl 3.0	18 Ar -
19 K 0.8	20 Ca 1.0	21 Sc 1.3	22 Ti 1.5	23 V 1.6	24 Cr 1.6	25 Mn 1.5	26 Fe 1.8	27 Co 1.8	28 Ni 1.8	29 Cu 1.9	30 Zn 1.6	31 Ga 1.6	32 Ge 1.8	33 As 2.0	34 Se 2.4	35 Br 2.8	36 Kr -		
37 Rb 0.8	38 Sr 1.0	39 Y 1.2	40 Zr 1.4	41 Nb 1.6	42 Mo 1.8	43 Tc 1.9	44 Ru 2.2	45 Rh 2.2	46 Pd 2.2	47 Ag 1.9	48 Cd 1.7	49 In 1.7	50 Sn 1.8	51 Sb 1.9	52 Te 2.1	53 I 2.5	54 Xe -		
55 Cs 0.7	56 Ba 0.9	57-71 La-Lu 1.1-1.2	72 Hf 1.3	73 Ta 1.5	74 W 1.7	75 Re 1.9	76 Os 2.2	77 Ir 2.2	78 Pt 2.2	79 Au 2.4	80 Hg 1.9	81 Tl 1.8	82 Pb 1.8	83 Bi 1.9	84 Po 2.0	85 At 2.2	86 Rn -		
87 Fr 0.7	88 Ra 0.9	89-102 Ac-No 1.1-1.7																	

Figure 2-21 *The electronegativities of the elements. (After Linus Pauling, *The Nature of the Chemical Bond and the Structure of Molecules and Crystals; An Introduction to Modern Structural Chemistry*, 3rd ed., Cornell University Press, Ithaca, New York, 1960)*

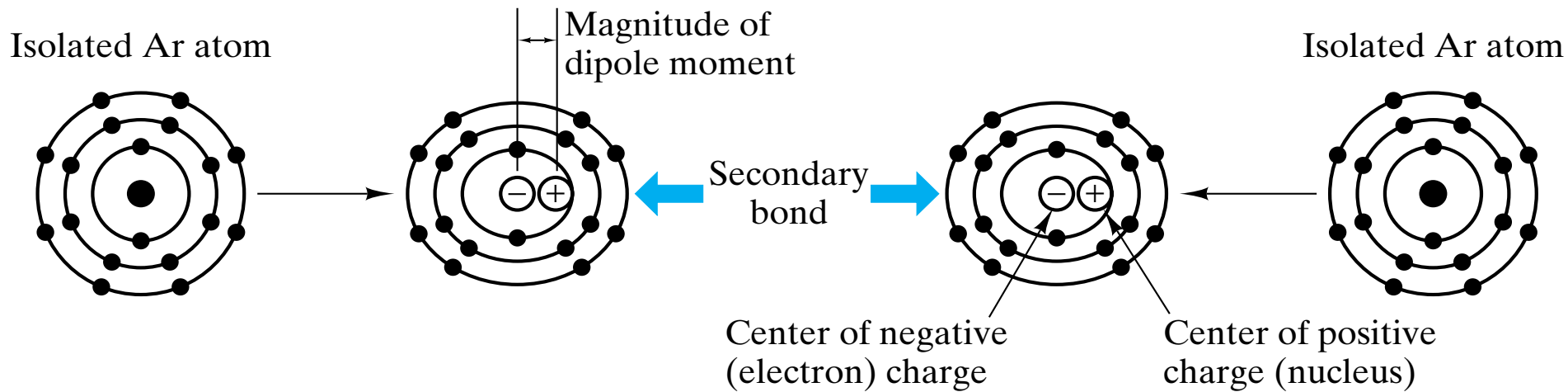


Figure 2-22 *Development of induced dipoles in adjacent argon atoms leading to a weak, secondary bond. The degree of charge distortion shown here is greatly exaggerated.*

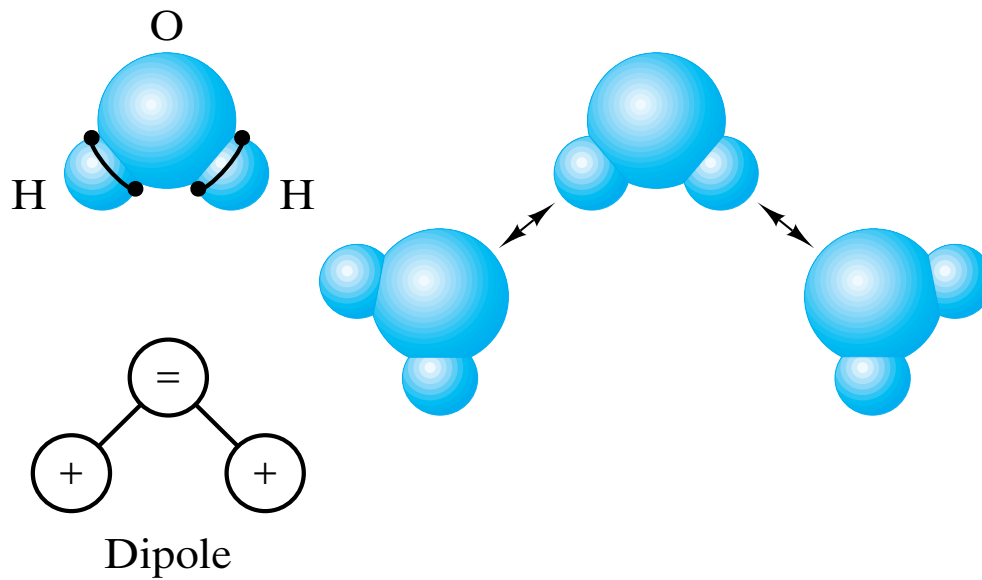


Figure 2-23 “Hydrogen bridge.” This secondary bond is formed between two permanent dipoles in adjacent water molecules. (From W. G. Moffatt, G. W. Pearsall, and J. Wulff, *The Structure and Properties of Materials, Vol. 1: Structures*, John Wiley & Sons, Inc., New York, 1964.)

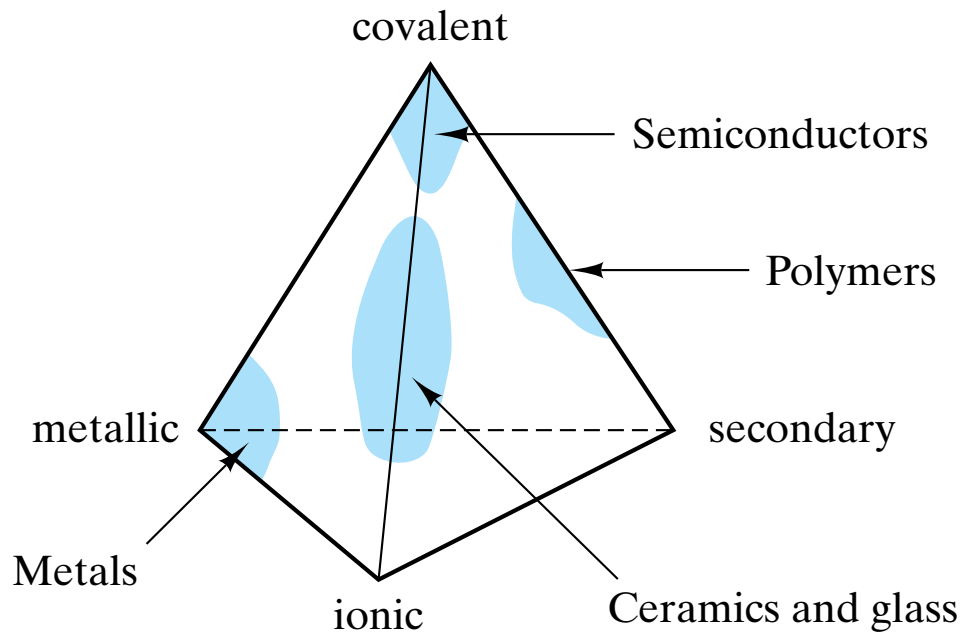


Figure 2-24 Tetrahedron representing the relative contribution of different bond types to the four fundamental categories of engineering materials (the three structural types plus semiconductors).

